Catalysis Today 419 (2023) 114152

Contents lists available at ScienceDirect

Catalysis Today

journal homepage: www.elsevier.com/locate/cattod

Hierarchical basic zeolites allow for the solvent-free synthesis of chromene derivatives

Monica J. Mendoza-Castro [1], Noemi Linares [*,2], Javier García-Martínez [*,3]

Laboratorio de Nanotecnología Molecular, Departamento de Química Inorgánica, Universidad de Alicante, Ctra. San Vicente-Alicante s/n, E-03690 San Vicente del Raspeig, Spain

ARTICLE INFO

Keywords:
Basic catalysis
Mesoporous zeolites
Surfactant-templating
Solvent-free synthesis
E-factor

ABSTRACT

The synthesis of 2-amino-chromene with excellent yields (82%) was achieved by utilizing basic hierarchical zeolites prepared by surfactant-templating as catalysts in a multicomponent reaction under solvent-free conditions. The use of these hierarchical zeolites more than doubles the activity of their microporous counterparts. These results highlight the superior diffusivity and performance of these basic hierarchical zeolites, which can be attributed to their well-developed intracrystalline mesoporosity, highly accessible and strong basic sites.

1. Introduction

Chromenes are oxy-containing bicyclic heterocycles [1], whose derivatives exhibit a myriad of pharmacological applications, such as antimicrobial [2], antioxidant [3], anti-inflammatory [4], β-secretase inhibition [5], antitrypanosomal [6], antidyslipidemic [7], anti-HIV [8], anti-depressant [9], and anticancer [3,10]. Traditional syntheses involve multi-step synthetic routes, whose intermediates must be isolated [11]. There is a significant interest to reduce the number of steps involved in their synthesis in order to decrease operational costs and the production of waste [12]. Organic bases can achieve this goal; however, it is highly desirable to replace these corrosive and difficult-to-separate bases with more benign heterogeneous catalysts [13].

While the use of zeolites as solid catalysts is widespread in many catalytic applications [14], their use in the synthesis of fine chemicals and pharmaceuticals is still limited [15]. This is partially due to the diffusion limitations caused by zeolites' narrow micropore network, which are especially severe in the synthesis of bulky organic molecules, such as the chromenes aforementioned [16]. We have recently realized the use of a mesoporous USY zeolite as a very attractive option for the production of active pharmaceutical compounds, which suffer diffusion limitation in conventional zeolites [17]. The incorporation of tuneable intracrystalline mesoporosity, while maintaining the key features of the zeolite, greatly enhances its activity in the conversion of bulky compounds.

Although, zeolites are mostly used as acid catalysts, there is an increasing interest in their use in base-catalyzed reactions [18]. Basic zeolites can be easily prepared by simple ion-exchange with alkali metal cations. These cations can be located at the ion-exchange sites of the zeolite or in the silanol groups (-Si-O–M, after they have been deprotonated) [19]. One of the main advantages of using basic zeolites in catalysis is the possibility to readily optimize their basicity for each reaction by using metallic cations of different electronegativity (in zeolites with $SiO_2/Al_2O_3 \cdot \leq 80$) [20]. Taking advantage of these properties, basic zeolites have been used to efficiently catalyze a variety of reactions including the Knoevenagel condensation, amide hydroxylation, one-pot multicomponent reactions (MCRs) and cycloaddition reactions, among others[13,19–26].

Here, we report the first use of a surfactant-templated zeolite as a basic catalyst in multicomponent synthesis. K- and Cs-ion-exchanged mesoporous zeolites prepared by this approach were evaluated for the synthesis of a 2-amino-chromene derivative, see Fig. 1, showing high activity and recyclability. Under solvent-free conditions, they show a 2–2.5-fold increase in yield over commercial USY zeolite, which leads up to 3-fold increase in Turn-Over-Numbers (TON). When our mesoporous zeolites are compared against a mesoporous ion-exchanged Al-MCM-41, a 200-fold increase in TON was observed, which points out the importance, not only of mesoporosity but also of strong basicity.

* Corresponding authors.
E-mail addresses: noemi.linares@ua.es (N. Linares), j.garcia@ua.es (J. García-Martínez).
[1] https://orcid.org/0000-0002-8810-0174
[2] https://orcid.org/0000-0001-9376-2984
[3] https://orcid.org/0000-0002-7089-4973

https://doi.org/10.1016/j.cattod.2023.114152
Received 12 January 2023; Received in revised form 29 March 2023; Accepted 6 April 2023
Available online 7 April 2023

2. Experimental

2.1. Materials

USY zeolite (CBV780 with molar ratio Si/Al = 40, as indicated by the supplier), was provided by Zeolyst®. Hexadecyltrimethylammonium bromide (CTAB) (98%), tetraethyl orthosilicate (TEOS), and small beads of sodium hydroxide (>98%) were purchased from Sigma-Aldrich. $AlCl_3$ was obtained from Fluka. The reactants employed in the catalytic tests, i.e. benzaldehyde (99%), malononitrile (99%), and 1-naphthol, were used as received from Sigma-Aldrich without further purification.

2.2. Synthesis of the mesoporous zeolite

The preparation of the surfactant-templated mesoporous zeolites was carried out by first dissolving CTAB (0.5 g) in 40 mL of aqueous 94 mM NaOH. To this mixture, 1 g of CBV780 zeolite was added and the resultant slurry was stirred at RT for 10 min. The surfactant-templating process was performed under static conditions by allowing the zeolite to remain in contact with the alkaline surfactant solution for 6 h at 30 °C. Calcination of the samples was carried out in air at 550 °C for 5 h (2 °C min^{-1}). A detailed description of the synthesis procedure can be found elsewhere [27].

2.3. Synthesis of the Al-MCM-41

The preparation of the Al-MCM-41 with a theoretical Si/Al ratio of 40 was performed by adapting the synthesis reported in [28]. First, 3.49 g of CTAB were dissolved under stirring (750 rpm) in an ammoniacal aqueous solution (320.5 mL of H_2O and 14.10 mL of NH_4OH (30%)). Once the CTAB was dissolved, 0.28 g of $AlCl_3$ and 18.6 mL of TEOS were added to this mixture, which was kept under stirring (750 rpm) at room temperature for 3 h. Then a hydrothermal treatment was carried out at 100 °C for 24 h. Calcination of the samples was carried out in air at 550 °C for 5 h (2 °C min^{-1}).

2.4. Ion-exchange of the catalysts

Aqueous MNO_3 solutions (M = K, or Cs) were used for ion-exchange to obtain the K- and Cs-form of the various catalysts (USY, Meso-USY, and Al-MCM-41). Ion-exchange was repeated five times at 70 °C for 2 h with 0.5 M MNO_3 solutions using a solution-to-catalyst ratio of 20 mL/g. The catalysts were washed twice with plenty of deionized water and dried overnight at 110 °C.

2.5. Samples characterization

The morphology of the catalysts was investigated by transmission electron microscopy (TEM) using a JEM-2010 microscope (JEOL, 200 kV, 0.14 nm of resolution). The samples were embedded in a Spurr resin and cut into slices 80 nm thin using an RMC-MTXL ultramicrotome (Boeckeler Instruments, Tucson, AZ). These slices were then displayed on a grid to observe by TEM the cross-sections of the zeolites before and after the introduction of the mesoporosity and the metallic cations. The digital analysis of the TEM micrographs was performed using Gatan DigitalMicrographTM 1.80.70 for GMS 1.8.

The porous texture of the samples was characterized by N_2 gas adsorption at 77 K in an AUTOSORB-6 apparatus. The samples were previously degassed for 8 h at 250 °C at 5 × 10^{-5} bars. Adsorption data were analyzed using the software QuadraWinTM (version 6.0) of Quantachrome Instruments. Cumulative pore volumes and pore-size distribution curves were calculated using the DFT method (cylinder pore, NL-DFT adsorption branch model). The total pore volume was obtained at the plateau of the cumulative adsorption pore volume plot at a relative pressure (P/P_0) of 0.95. Micropore volume was determined from the same plot at a pore size < 2 nm, and mesopore volume was calculated by subtracting the micropore volume from the total pore volume, as described elsewhere [29].

The crystallinity of the materials was characterized by X-ray powder diffraction (XRD) in the wide-angle region from 5 to 60 degrees 2θ range using a scanning velocity of 1° min^{-1}; in a SEIFERT 2002 apparatus using a CuK_α (1.5418 Å) radiation. A known amount of graphite (10 wt %) was mixed with the zeolite before analysis to be used as internal standard to compare the crystallinity of the different samples (see the peak corresponding to the graphite at ca. 26° 2θ).

To study the basic species formed in the studied materials Cs- and K-containing zeolites were analyzed via X-ray photoelectron spectroscopy (XPS, K-Alpha +, Thermo Scientific) with the AlKα radiation (1486.6 eV) at a high-resolution of 0.1 eV step. The binding energy was calibrated to 284.6 eV (C 1 s). The K 2p, Cs 3d and O 1 s peaks were fitted at a Gaussian–Lorentz peak shape (G:L ratio = 60:40) and Shirley background function.

The elemental distribution of the metallic cations in the crystals was studied by scanning transmission electron microscopy-energy dispersive

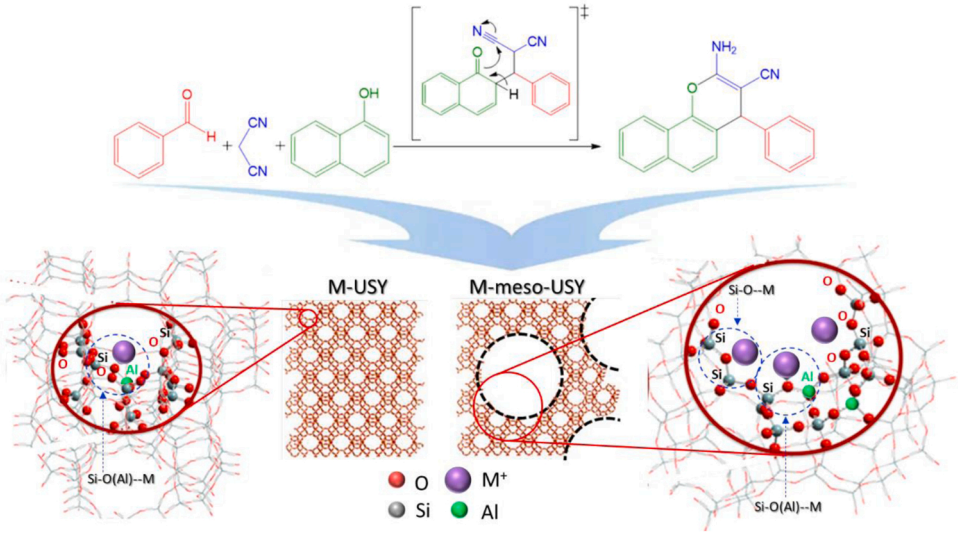

Fig. 1. Schematic representation of the MCR synthesis of the 2-amino-chromene derivative by coupling benzaldehyde, malononitrile and α-naphthol in the presence of a surfactant-templated basic zeolite. The two different types of basic sites in the catalysts are also depicted.

X-ray spectrometry (STEM-EDX) in ultramicrotomed samples. A FEI Talos F200X high-resolution microscope with 200 kV FEG gun, 4 simultaneous EDX detectors, EELS, and 4 STEM detectors (HAADF, DF1, DF2, BF) was employed for the analysis. The elemental composition was determined by inductively coupled plasma optical emission spectroscopy (ICP-OES). The samples were dissolved in a mixture of 3,5 mL HCl + 1 mL HNO_3 + 1 mL HF + 5 mL H_3BO_3 (5%), digested in a microwave (260 ºC, 45 bar) and filtered off (0.45 μm) prior to analysis. This treatment is able to entirely dissolve the samples.

The identification of the synthesized chromene was by ^{1}H and ^{1}H-COSY nuclear magnetic resonance (NMR). The spectra were recorded with a Bruker Spectrospin Avance 400 spectrometer with dimethylsulfoxide (DMSO)-d6 as solvent and tetramethylsilane (TMS) as internal standard. ^{1}H-COSY experiment was made in the same conditions that 1D but with a coupling pulse that tilts the nuclear spin by 90°. All chemical shifts are reported as δ (ppm), and coupling constants (J) are given in Hz.

2.6. Catalytic evaluation

(I) Knoevenagel condensation. The reactions were performed as follows: 2 mmol of malononitrile was stirred with 192 μl of benzaldehyde in a glass vessel containing 50 mg of the catalyst for the reaction. The vials were tightly closed and transferred into an aluminum heating block preheated to 80 ºC. The mixture was stirred (400 rpm) at this temperature for different reaction times. The reaction mixture was cooled down, washed with ethanol, and centrifuged. Products were identified by comparing the retention time with that of pure samples in gas chromatography coupled to an FID detector (GC-FID).

(II) One-pot, multi-component reaction for the synthesis of naphthopyrans. 0.4 mmol of each reactant (benzaldehyde, malononitrile, and 1-naphthol, all (99%)) and 10 mg of the tested catalyst were added to a 1.5 mL glass vessel. The vials were tightly closed and transferred into an aluminum heating block preheated at 100 ºC. The mixture was magnetically stirred (400 rpm), and heated at 100 ºC for different times. The crude mixture was cooled down, diluted in dichloromethane and separated by centrifugation. In the recyclability tests, after each reaction cycle was finished, the catalysts were recovered by centrifugation, thoroughly washed with dichloromethane and ethanol and reused by the addition of a new reaction mixture. Products were confirmed using ^{1}H NMR and ^{1}H-^{1}H COSY and the reaction was followed by comparing the retention time with that of pure samples in gas chromatography coupled to an FID detector (GC-FID).

In both cases, experiments were performed three times to ensure the reproducibility of the results.

3. Results and discussion

The hierarchical nature of the catalysts was confirmed by N_2 adsorption, as shown in Fig. 2. The surfactant-templating treatment allows for the development of a high amount of intracrystalline mesoporosity (0.54 $cm^3\ g^{-1}$) while a high amount of microporosity (0.13 $cm^3\ g^{-1}$) and crystallinity (81%) of the original zeolite was preserved (Fig. 2a-b and Table S1). The incorporation of the metallic cations (K^+ and Cs^+) only slightly modifies the textural properties of the Na,H-containing zeolites (25% reduction in microporosity and maintaining of the mesoporosity, Fig. S1 and Table S1). The newly created mesopore system is homogeneously distributed throughout the crystal, as can be observed by the TEM micrographs of ultramicrotomed samples before (Fig. S2a) and after (Fig. S2b-e) the treatment.

The loading and distribution of the metallic cations in the samples were studied by ICP and STEM-EDX, respectively. The amount of metal incorporated to the zeolites ranges between 0.15 and 0.22 mmol/g for both metals (Table S1). Under the same conditions, mesoporous samples incorporate a higher amount of cations (ca. 25% higher loading), which is likely due to the enhanced accessibility of these voluminous cations to the exchange sites [30] and/or the formation of new sites (after surfactant-templating the M^+/Al ratio reaches values near to 1 vs ca. 0.7 for the microporous zeolite, see Table S1) [31]. The higher diffusion limitations of the Cs^+ cation versus K^+ could be responsible of their different distributions throughout the zeolite crystal, as shown in Fig. 2d. While the EDX mapping of K in both zeolites (original and mesoporous) displays an even distribution of the metal through the whole crystal, Cs-ion-exchanged zeolites show opposite results. Both zeolites show a Cs-enrichment on the exterior surface (Fig. 2d). This irregular distribution of Cs is more evident in the microporous zeolite, which shows a lower amount of the cation in the interior of the crystal. The chemical nature of the Cs^+ and K^+ species in the ion-exchanged zeolites was studied by XPS (Fig. 2c). The incorporation of the cations in the microporous zeolite produces two bands in the Cs $3d_{5/2}$ and K 2p XPS spectra, which are due to the cations in the ion-exchange sites of the zeolite (Si-O(Al)—M). However, in the mesoporous zeolites two contributions were observed in each of these bands, thus suggesting the presence of the cations in at least two different chemical environments (Fig. 1). While the band at higher binding energy (BE ca. 723.5 eV) is associated to the Cs^+ ions in the exchange sites of the zeolite (Si-O(Al)–Cs), the assignment of the specie at lower BE (ca. 721.7 eV) is more challenging. Its location at lower BE rules out the possibility of Cs_2O formation, as this would appear at higher values [32,33]. On the other hand, as elsewhere reported [19,31], Cs^+ ions can be located in the deprotonated silanol groups of the zeolite framework (Si-O–Cs); although this would require a high pH, which is not the case during the ion-exchange procedure. However, the incorporation of mesoporosity takes place at high pH in the presence of Na^+, which could favour the formation of (Si-O–Na) species [31]. The subsequent ion-exchange would then produce this new type of basic sites (Si-O–Cs). The same conclusions can be drawn from the analysis of the K 2p spectra.

O 1s XPS spectra were determined to get deeper insight of the basicity of the zeolites, because their BE values have shown to be a good proxy of their basic behaviour [21]. As basicity increases, BE shifts to lower values, because the outermost electrons are less bounded to the oxygen atoms. With this in mind, and according to the XPS results shown in Fig. 2c and Table S2, we conclude that Cs- and K-ion-exchanged mesoporous zeolites are more basic than their microporous counterparts, as the main band of the O 1s XPS spectra are shifted, in both cases, to lower BE values (see Table S2). This is consistent with the presence of (Si-O–M) species in the zeolite because, as reported elsewhere [19], they show a higher basic strength than the usual ion-exchange sites.

In order to analyze the potential of these materials as basic catalysts, they were tested first for the Knoevenagel condensation between benzaldehyde and malononitrile, a well-known reaction used as benchmark for this kind of catalysts. For both cations, mesoporous zeolites show improved yields towards the production of benzylidenemalononitrile, the desired product (see Fig. S3). Due to the small size of the reagents and product (critical size of the product: 0.49 nm), they can easily enter the micropore system of the zeolite (pore size of FAU: 0.74 nm).. However, as described elsewhere, the external surface area plays a key role in this reaction even in cases where small reagents are involved [34]. This explains why the incorporation of mesoporosity produces an enhancement of the zeolites' catalytic activity. Moreover, the incorporation of mesoporosity by surfactant-templating produces new and more basic Cs^+ and K^+ sites (Si-O–M), which agrees with the higher catalytic activity of these materials, even using compounds with no diffusional limitations.

Subsequently, both conventional and hierarchical zeolites were tested as catalysts for the multicomponent synthesis of the 2-amino-chromene derivative shown in Fig. 1, under solvent-free conditions (see Section 2.6 for details). The desired 2-amino-chromene was identified, by 1 and 2D NMR (Fig. S4 and S5), as the only product of the reaction, as expected for this highly selective MCR. In the ^{1}H–^{1}H-COSY experiment (2D NMR), all the hydrogen atoms coupled to each other, creating a diagonal line on the graph as a reflective plane. This is

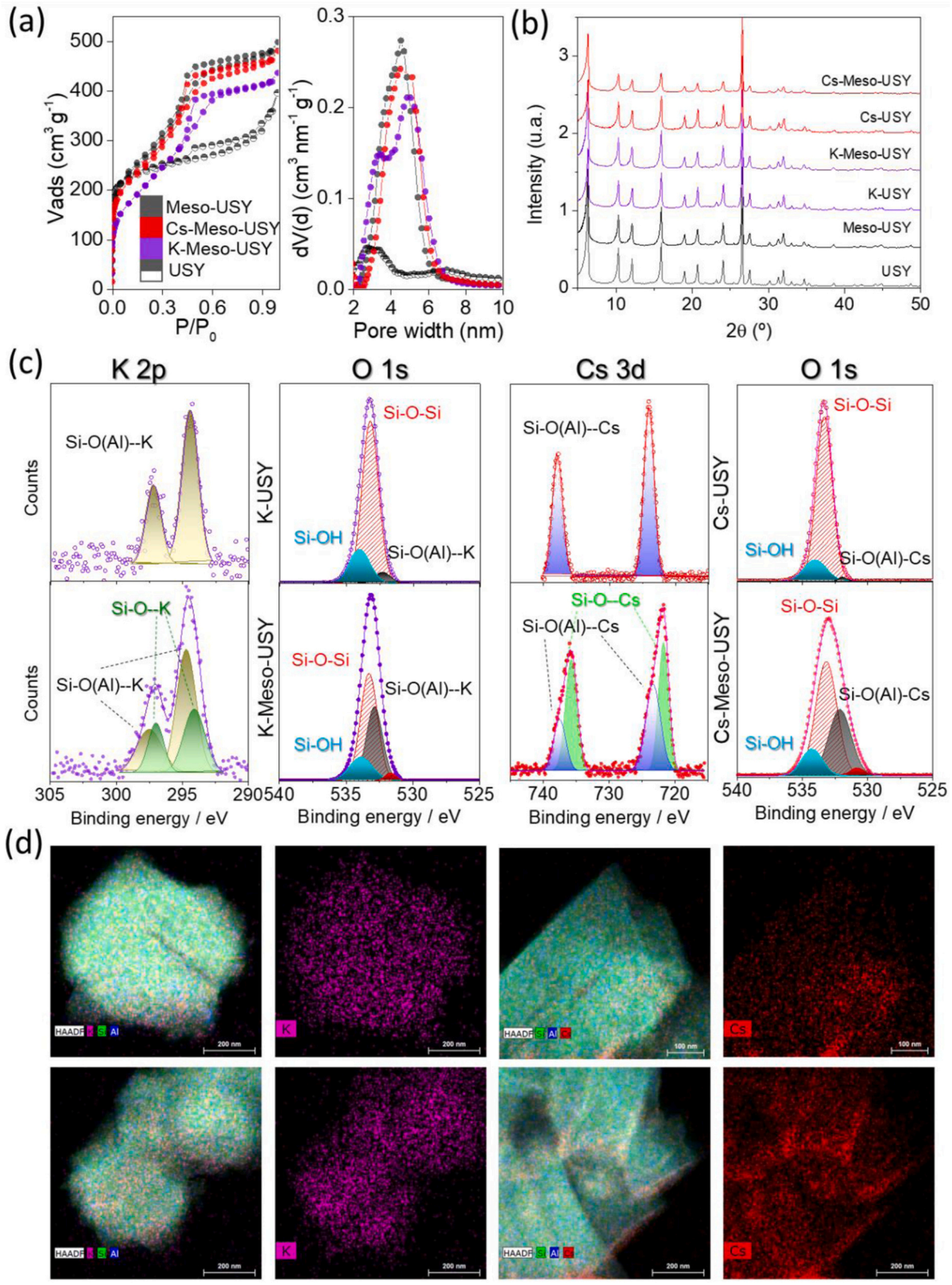

Fig. 2. (a) N_2 sorption isotherms at 77 K of the original and surfactant-templated zeolites before and after the incorporation of the metallic cations (samples are labelled in the legend) and the derived pore size distributions calculated from the adsorption branch by the NL-DFT method. (b) X-ray diffraction patterns of the same samples. (c) X-ray photoelectron spectra for the microporous (top) and mesoporous (bottom) zeolites with K (left) and Cs (right). (d) STEM-EDX elemental mappings of (top row) microporous original USY zeolite and (bottom row) the mesoporous counterpart. The two images on the left correspond to K-ion-exchanged zeolites and the two on the right to Cs-ion-exchanged ones. Color coding: Si (green), Al (blue), K^+ (purple), and Cs^+ (red).

typically associated with compounds that are free from impurities, as impurities would cause additional peaks or disruptions in the pattern [35]. In all cases, the surfactant-templated zeolite exhibited higher catalytic activity than the conventional zeolite (see Fig. 3a). After 3.5 h of reaction, the metal ion-exchanged mesoporous zeolites yield ca. 2–2.5 more chromene than their microporous counterparts (Fig. 3a). The higher activity of the mesoporous zeolites is also evidenced by the 4-fold increase in the pseudo-first-order kinetic rate constant, k′, (Fig. 3b). As control experiments, both H- and Na-containing zeolites were also tested (Fig. 3c). As expected, the acid zeolites do not show much activity for this reaction, while the presence of Na^+ slightly increase their performance. Based on these results, we conclude that K- and Cs-Meso-USY show a superior performance due to the combination of both strong basicity and improved accessibility. More specifically, the sample Cs-Meso-USY, which contains the strongest basic sites (due to the lowest electronegativity of the Cs^+) [23] and plenty of mesoporosity yielded the best results (Yield = 82%, $k' = 0.47\ h^{-1}$).

Once the activity was evaluated, we tested the recyclability of all the basic zeolites. Contrary to what was observed for acid-catalyzed reactions [17], all solids preserve most of their initial activity after 4 catalytic cycles, as they lack the acid sites which cause the formation of coke, one of the mechanisms that leads to catalyst deactivation. The mesoporous zeolites converted much substrate than the microporous ones during the 4 recycles. More specifically, the best performing catalyst, the Cs-ion-exchanged mesoporous zeolite, produced a total amount of 1.23 mmol of 2-amino-chromene after the 4 cycles, while the microporous zeolite only yielded a bit more than half of this amount (0.69 mmol).

Further evidence supporting the need of strong basic sites is demonstrated by the lower activity of K- or Cs-ion-exchanged Al-MCM-41 catalysts in comparison to K- and Cs-Meso-USY. This can be attributed to the existence of numerous but weaker basic sites. In fact, the XPS spectra of the Al-MCM-41 materials do not exhibit the presence of the strongest Si-O–M sites (refer to Fig. S6) [25]. Correspondingly, under the same reaction conditions, their performances are the lowest, TON Cs-Al-MCM-41 = 240 vs Cs-Meso-USY = 12000 (Fig. 3f). Taking all these observations into account, our results show that surfactant-templated zeolites, with their unique combination of well-defined mesoporosity and easily accessible ion-exchange and siloxy sites, are very promising catalysts for the immobilization of metallic cations able to base-catalyzed the synthesis of the bulky derivatives involved in both fine-chemical and pharmaceutical production processes.

One important aspect that we would like to highlight is that all the reactions were carried out without solvent. This was possible thanks to the very open structure of our catalysts. This allowed us to drastically reduce the E-factor (kg waste / kg product) reported for this reaction. As shown in Table S3, our mesoporous zeolites present E-factors below 1.5, while most of the reported synthesis are above 14, meaning more than a 10-fold reduction of wastes in our process. By using our catalysts, the E-factor can be reduced to levels more typical of bulk chemical production (Table S3).

4. Conclusions

The incorporation of mesoporosity in USY zeolite followed by ion-exchange with alkaline cations (K^+ and Cs^+) results in a significant increase in activity for the multicomponent synthesis of chromene derivatives. More specifically, surfactant-templated hierarchical USY zeolites feature well-defined mesoporosity, easily accessible ion-exchange sites, and siloxy-cation ion pairs (Si-O–M), making them superior base catalysts for the production of bulky molecules compared to

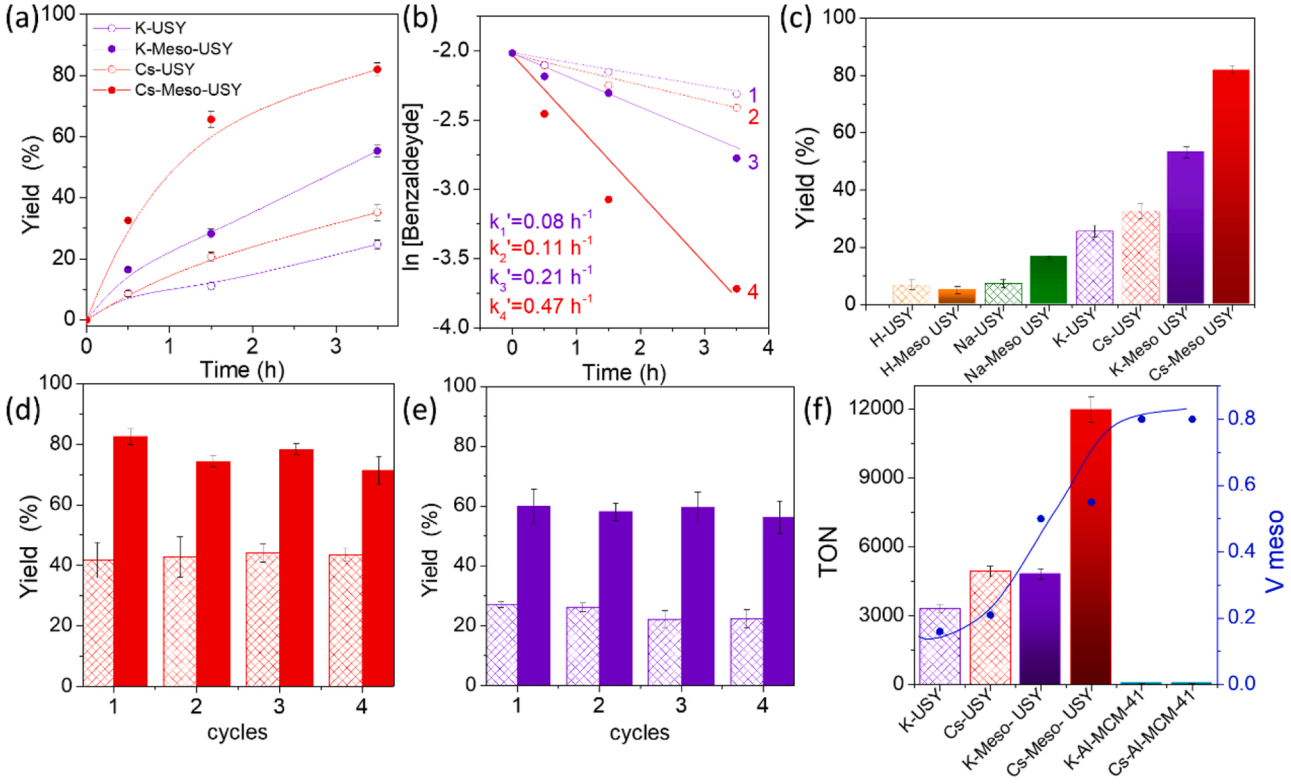

Fig. 3. Catalytic performance of the different catalysts in the multicomponent synthesis of 2-amino-chromene: (a) Yield of the product catalyzed by Cs- (red) and K-ion-exchanged (purple) mesoporous (filled symbols, solid lines) and microporous (empty symbols, doted lines) zeolites. (b) Calculation of the pseudo-first order kinetic rate constants, k′, for the same catalysts. (c) Yield obtained by a series of zeolites prepared introducing different cations, with and without mesoporosity. Recyclability tests for the (d) Cs- and (e) K-ion-exchanged zeolites. (f) Catalytic activity of the Cs- and K-ion-exchanged zeolites and a totally mesoporous catalyst, namely Al-MCM-41.

conventional zeolites. In particular, Cs^+ ion-exchanged hierarchical USY zeolite exhibits a 4-fold increase in the pseudo-first-order kinetic rate constant compared to their microporous counterparts for the solvent-free multicomponent synthesis of a 2-amino-chromene derivative. Remarkably, our catalysts demonstrate excellent performance even in the absence of solvent, leading to a substantial reduction in the E-factor (up to 0.40). The ability to use the surfactant-templating approach to develop strong catalytic basic sites while simultaneously enhancing the diffusion characteristics of zeolites presents an attractive option for designing novel basic catalysts with superior catalytic performance for the sustainable synthesis of bulky molecules.

Funding sources

European Union's Horizon 2020 research and innovation programme under grant agreement No 872102. Ministry of Science and Innovation and AEI/FEDER, UE project ref. PID2021-128761OB-C21. Generalitat Valenciana PhD fellowship ref. GRISOLIAP/2020/165.

CRediT authorship contribution statement

M.J.M. synthesized the materials, conducted morphological and structural characterizations and the catalytic evaluation. M.J.M., N.L. and J.G.M. realized the corresponding analysis. The manuscript was written through contributions of all authors. All authors have given approval to the final version of the manuscript. N.L. and J.G.M. conceived the idea and supervised the study.

Declaration of Competing Interest

The authors declare the following financial interests/personal relationships which may be considered as potential competing interests: Javier Garcia Martinez reports financial support was provided by W*R* Grace and Co. Javier Garcia Martinez reports a relationship with W*R* Grace and Co that includes: consulting or advisory. Javier Garcia Martinez has patent licensed to W*R* Grace and Co.

Data Availability

Data will be made available on request.

Acknowledgment

This project has received funding from the European Union's Horizon 2020 research and innovation programme under grant agreement No 872102. The authors thank the Spanish Ministry of Science and Innovation and AEI/FEDER, UE for funding through the project ref. PID2021–128761OB-C21. M.J.M. thanks the Generalitat Valenciana for a PhD fellowship (GRISOLIAP/2020/165).

Appendix A. Supporting information

Supplementary data associated with this article can be found in the online version at doi:10.1016/j.cattod.2023.114152.

References

[1] R. Pratap, V.J. Ram, Natural and synthetic chromenes, fused chromenes, and versatility of dihydrobenzo[h]chromenes in organic synthesis, Chem. Rev. 114 (2014) 10476–10526, https://doi.org/10.1021/CR500075S/ASSET/IMAGES/MEDIUM/CR-2014-00075S_0019.GIF.

[2] M. Nikpassand, L. Fekri, H. Badri, L. Asadpour, Synthesis and antimicrobial activity of Mono, Bis and Tris 2-Amino-4HChromenes, Lett. Org. Chem. 12 (2015) 685–692, https://doi.org/10.2174/1570178612101511021516 56.

[3] P. Anaikutti, M. Selvaraj, J. Prabhakaran, T. Pooventhiran, T.C. Jeyakumar, R. Thomas, P. Makam, Indolyl-4H-chromenes: multicomponent one-pot green synthesis, in vitro and in silico, anticancer and antioxidant studies, J. Mol. Struct. 1266 (2022), 133464, https://doi.org/10.1016/J.MOLSTRUC.2022.133464.

[4] P. Gebhardt, K. Dornberger, F.A. Gollmick, U. Gräfe, A. Härtl, H. Görls, B. Schlegel, C. Hertweck, Quercinol, an anti-inflammatory chromene from the wood-rotting fungus Daedalea quercina (Oak Mazegill), Bioorg. Med. Chem. Lett. 17 (2007) 2558–2560, https://doi.org/10.1016/J.BMCL.2007.02.008.

[5] V. Bhaskar, R. Chowdary, S.R. Dixit, S.D. Joshi, Synthesis, molecular modeling and BACE-1 inhibitory study of tetrahydrobenzo[b] pyran derivatives, Bioorg. Chem. 84 (2019) 202–210, https://doi.org/10.1016/J.BIOORG.2018.11.023.

[6] J.M. Batista, A.A. Lopes, D.L. Ambrósio, L.O. Regasini, M.J. Kato, V.D.S. Bolzani, R. M.B. Cicarelli, M. Furlan, Natural chromenes and chromene derivatives as potential anti-trypanosomal agents, Biol. Pharm. Bull. 31 (2008) 538–540, https://doi.org/10.1248/BPB.31.538.

[7] K.V. Sashidhara, J.N. Rosaiah, G. Bhatia, J.K. Saxena, Novel keto-enamine Schiffs bases from 7-hydroxy-4-methyl-2-oxo-2H-benzo[h] chromene-8,10-dicarbaldehyde as potential antidyslipidemic and antioxidant agents, Eur. J. Med. Chem. 43 (2008) 2592–2596, https://doi.org/10.1016/J.EJMECH.2007.10.029.

[8] Y. Wang, S.X. Huang, P. Xia, Y. Xia, Z.Y. Yang, N. Kilgore, S.L. Morris-Natschke, K. H. Lee, Anti-AIDS agents 72. Bioisosteres (7-carbon-DCKs) of the potent anti-HIV lead DCK, Bioorg. Med. Chem. Lett. 17 (2007) 4316–4319, https://doi.org/10.1016/J.BMCL.2007.05.026.

[9] N.E. Vergel, J.L. López, F. Orallo, D. Viña, D.M. Buitrago, E. del Olmo, J.A. Mico, M.F. Guerrero, Antidepressant-like profile and MAO-A inhibitory activity of 4-propyl-2H-benzo[h]-chromen-2-one, Life Sci. 86 (2010) 819–824, https://doi.org/10.1016/J.LFS.2010.04.001.

[10] T.C. Braga, M.M. Silva, E.O.O. Nascimento, E.C. Dantas da Silva, Y. de Freitas Rego, M. Mandal, Z. Alves de Souza, A.L. Tasca Góis Ruiz, J. Ernesto de Carvalho, F. T. Martins, I.M. Figueiredo, T. Mendonça de Aquino, C. Moreira da Silva, B. Mandal, G. Brahmachari, J.C. Caldas Santos, Â. de Fátima, Synthesis, anticancer activities and experimental-theoretical DNA interaction studies of 2-amino-4-phenyl-4H-benzo[h]chromene-3-carbonitrile, Eur. J. Med. Chem. Rep. 4 (2022), 100030, https://doi.org/10.1016/J.EJMCR.2022.100030.

[11] J. Bloxham, C.P. Dell, C.W. Smith, Preparation of some new benzylidenemalononitriles by an SNAr reaction: Application to naphtho[1,2-b] pyran synthesis, Heterocycles 38 (1994) 399–408, https://doi.org/10.3987/com-93-6594.

[12] R.C. Cioc, E. Ruijter, R.V.A. Orru, Multicomponent reactions: advanced tools for sustainable organic synthesis, Green. Chem. 16 (2014) 2958–2975, https://doi.org/10.1039/C4GC00013G.

[13] M.J. Climent, A. Corma, S. Iborra, Homogeneous and heterogeneous catalysts for multicomponent reactions, RSC Adv. 2 (2011) 16–58, https://doi.org/10.1039/C1RA00807B.

[14] M. Shamzhy, M. Opanasenko, P. Concepción, A. Martínez, New trends in tailoring active sites in zeolite-based catalysts, Chem. Soc. Rev. 48 (2019) 1095–1149, https://doi.org/10.1039/c8cs00887f.

[15] F.G. Cirujano, Engineered MOFs and enzymes for the synthesis of active pharmaceutical ingredients, ChemCatChem 11 (2019) 1–16, https://doi.org/10.1002/cctc.201900131.

[16] J. García-Martínez, K. Li, Mesoporous Zeolites, Wiley-VCH Verlag GmbH & Co. KGaA, Weinheim, Germany, 2015. https://doi.org/10.1002/9783527673957.

[17] N. Linares, F.G.F.G. Cirujano, D.E. De Vos, J. García-Martínez, Surfactant-templated zeolites for the production of active pharmaceutical intermediates, Chem. Commun. 55 (2019) 12869–12872, https://doi.org/10.1039/c9cc06696a.

[18] J. Weitkamp, M. Hunger, U. Rymsa, Base catalysis on microporous and mesoporous materials: recent progress and perspectives, Microporous Mesoporous Mater. 48 (2001) 255–270, https://doi.org/10.1016/S1387-1811(01)00366-3.

[19] T.C. Keller, K. Desai, S. Mitchell, J. Pérez-Ramírez, Design of base zeolite catalysts by alkali-metal grafting in alcoholic media, ACS Catal. 5 (2015) 5388–5396, https://doi.org/10.1021/acscatal.5b00761.

[20] T.C. Keller, S. Isabettini, D. Verboekend, E.G. Rodrigues, J. Pérez-Ramírez, Hierarchical high-silica zeolites as superior base catalysts, Chem. Sci. 5 (2014) 677–684, https://doi.org/10.1039/C3SC51937F.

[21] L. Martins, W. Hölderich, D. Cardoso, Methylammonium-FAU zeolite: Investigation of the basic sites in base catalyzed reactions and its performance, J. Catal. 258 (2008) 14–24, https://doi.org/10.1016/J.JCAT.2008.05.018.

[22] S. Inagaki, K. Thomas, V. Ruaux, G. Clet, T. Wakihara, S. Shinoda, S. Okamura, Y. Kubota, V. Valtchev, Crystal growth kinetics as a tool for controlling the catalytic performance of a FAU-type basic catalyst, ACS Catal. 4 (2014) 2333–2341, https://doi.org/10.1021/cs500153e.

[23] R.J. Davis, New perspectives on basic zeolites as catalysts and catalyst supports, J. Catal. 216 (2003) 396–405, https://doi.org/10.1016/S0021-9517(02)00034-9.

[24] G. Busca, Acidity and basicity of zeolites: a fundamental approach, Microporous Mesoporous Mater. 254 (2017) 3–16, https://doi.org/10.1016/J.MICROMESO.2017.04.007.

[25] J. Liang, Z. Liang, R. Zou, Y. Zhao, J. Liang, Y.L. Zhao, Z. Liang, R. Zou, Heterogeneous catalysis in zeolites, mesoporous silica, and metal–organic frameworks, Adv. Mater. 29 (2017) 1701139, https://doi.org/10.1002/ADMA.201701139.

[26] V. Verdoliva, M. Saviano, S. De Luca, Zeolites as acid/basic solid catalysts: recent synthetic developments, Catal Vol. 9 (2019) 248, https://doi.org/10.3390/CATAL9030248.

[27] A. Chawla, N. Linares, J.D. Rimer, J. García-Martínez, Time-Resolved dynamics of intracrystalline mesoporosity generation in USY zeolite, Chem. Mater. 31 (2019) 5005–5013, https://doi.org/10.1021/acs.chemmater.9b00435.

[28] J. Garcia-Martinez, N. Linares, S. Sinibaldi, E. Coronado, A. Ribera, Incorporation of Pd nanoparticles in mesostructured silica, Microporous Mesoporous Mater. 117 (2009) 170–177, https://doi.org/10.1016/j.micromeso.2008.06.038.

[29] M.J. Mendoza-Castro, E. Serrano, N. Linares, J. García-Martínez, Surfactant-templated zeolites: from thermodynamics to direct observation, Adv. Mater. Interfaces 8 (2021) 2001388, https://doi.org/10.1002/admi.202001388.
[30] D. Verboekend, T.C. Keller, S. Mitchell, J. Pérez-Ramírez, Hierarchical FAU- and LTA-Type zeolites by post-synthetic design: a new generation of highly efficient base catalysts, Adv. Funct. Mater. 23 (2013) 1923–1934, https://doi.org/10.1002/adfm.201202320.
[31] T.C. Keller, E.G. Rodrigues, J. Pérez-Ramírez, Generation of basic centers in high-silica zeolites and their application in gas-phase upgrading of bio-oil, ChemSusChem 7 (2014) 1729–1738, https://doi.org/10.1002/CSSC.201301382.
[32] E. Díaz, E. Muñoz, A. Vega, S. Ordóñez, Enhancement of the CO_2 retention capacity of y zeolites by Na and Cs treatments: effect of adsorption temperature and water treatment, Ind. Eng. Chem. Res. 47 (2008) 412–418, https://doi.org/10.1021/IE070685C/ASSET/IMAGES/LARGE/IE070685CF00006.JPEG.
[33] X. Wang, G. Zhao, L. Miao, Z. Hong, Y. Huang, Z. Zhu, Side-chain alkylation of toluene with methanol over cesium-ion-exchanged zeolite LSX and X catalysts, N. J. Chem. 46 (2022) 1034–1041, https://doi.org/10.1039/D1NJ04239D.
[34] D. Verboekend, T.C. Keller, S. Mitchell, J. Pérez-Ramírez, Hierarchical FAU- and LTA-Type zeolites by post-synthetic design: a new generation of highly efficient base catalysts, Adv. Funct. Mater. 23 (2013) 1923–1934, https://doi.org/10.1002/ADFM.201202320.
[35] D. Marion, Reprint of "Application of phase sensitive two-dimensional correlated spectroscopy (COSY) for measurements of 1H–1H spin–spin coupling constants in proteins, Biochem. Biophys. Res. Commun. 425 (2012) 519–526, https://doi.org/10.1016/j.bbrc.2012.08.018.